Article

Bismuth Telluride Hexagonal Nanoplatelets and Their Two-Step Epitaxial Growth

Weigang Lu, Yong Ding, Yuxi Chen, Zhong Lin Wang, and Jiye Fang

J. Am. Chem. Soc., **2005**, 127 (28), 10112-10116• DOI: 10.1021/ja052286j • Publication Date (Web): 24 June 2005

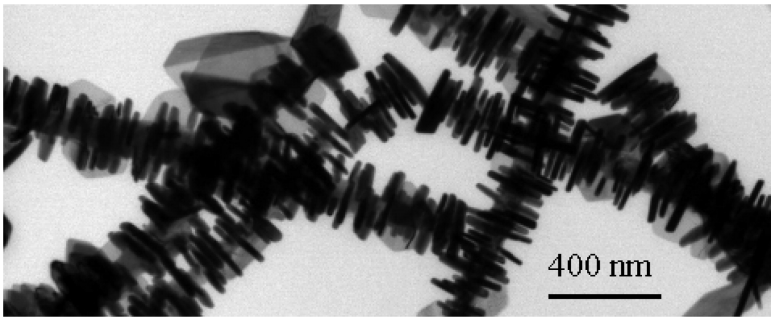

J|A|C|S
ARTICLES
Published on Web 06/24/2005

Bismuth Telluride Hexagonal Nanoplatelets and Their Two-Step Epitaxial Growth

Weigang Lu,[†] Yong Ding,[‡] Yuxi Chen,[†] Zhong Lin Wang,*[,‡] and Jiye Fang*[,†]

Contribution from the Department of Chemistry and Advanced Materials Research Institute, University of New Orleans, New Orleans, Louisiana 70148, and School of Materials Science and Engineering, Georgia Institute of Technology, Atlanta, Georgia 30332

Received April 8, 2005; E-mail: jfang1@uno.edu; zhong.wang@mse.gatech.edu

Abstract: We report a synthesis of discrete, single-crystal, defect-free, and hexagonal Bi_2Te_3 nanoplatelets using a high-temperature organic solution approach, and we demonstrate a two-step epitaxial growth of the cylindrical strings of Bi_2Te_3 nanoplatelets on the surface of the Te rod by packing them along *c*-axis in a top−bottom−top−bottom sequence. This type of building-up provides additional opportunity for the exploration of novel thermoelectric properties from such quantum-confined materials, in which the boundary scattering of phonons is anticipated to enhance.

Introduction

The challenge for realizing superior thermoelectric materials lies in the improvement of the thermoelectric figure of merit, i.e. simultaneous increase of electrical conductivity, increase of thermoelectric power, and decrease of thermal conductivity. Except for the skutterudite exploration,[1−5] efforts for enhancing the thermoelectric figure of merit were alternatively made in the direction of reducing the dimensionality of typical materials into the nanoscale.[6−9] In fact, both theoretical calculations[6,10] and experimental investigations[8,11−13] have suggested an additional strategy to achieve a high thermoelectric figure of merit from low-dimensional materials due to both a higher density of states and an increased phonon scattering or reduced lattice thermal conductivity in low-dimensional systems.[14] Much larger enhancements in thermoelectric cooling efficiency are predicted in true quantum-confined systems because of the fact that a very small active region with a much shorter response time than those of bulk thermoelectric devices can be achieved and the fact that such nanostructures can offer opportunities to increase the boundary scattering of phonons at the barrier−well interfaces without as large an increase in electron scattering at the interface.[10,13,15,16]

Bismuth telluride (Bi_2Te_3) is one of the best thermoelectric materials with the highest figure of merit. As a typical thermoelectric material which has been most often used for decades due to its unique characteristics, the Bi_2Te_3 crystal has been transferred into low-dimensional scale through various wet chemical approaches, including hydrogen reduction,[17,18] precipitation from nonaqueous solution[19] and reverse micelles,[20] as well as other methods such as electrodeposited nanowires prepared from porous alumina[21−24] and intercalation/exfoliation routes.[25,26] To evaluate the transport and electronic properties of quantum-confined Bi_2Te_3 crystal, the next challenge is to manipulate specific nanostructures in which the boundary scattering of phonons is anticipated to increase. High-temper-

[†] University of New Orleans.
[‡] Georgia Institute of Technology.

(1) Sales, B. C.; Mandrus, D.; Williams, R. K. *Science* **1996**, *272*, 1325−1328.
(2) Tritt, T. M. *Science* **1999**, *283*, 804−805.
(3) Tritt, T. M. *Mater. Res. Soc. Symp. Proc.* **2002**, *691*, G1.1.1−G1.1.12.
(4) Nolas, G. S.; Morelli, D. T.; Tritt, T. M. *Annu. Rev. Mater. Sci.* **1999**, *29*, 89−116.
(5) Hsu, K. F.; Loo, S.; Guo, F.; Chen, W.; Dyck, J. S.; Uher, C.; Hogan, T.; Polychroniadis, E. K.; Kanatzidis, M. G. *Science* **2004**, *303*, 818−821.
(6) Hicks, L. D.; Dresselhaus, M. S. *Phys. Rev. B: Condens. Mater. Phys.* **1993**, *47*, 12727−12731.
(7) Hicks, L. D.; Harman, T. C.; Sun, X.; Dresselhaus, M. S. *Phys. Rev. B: Condens. Mater. Phys.* **1996**, *53*, 10493−10496.
(8) Dresselhaus, M. S.; Dresselhaus, G.; Sun, X.; Zhang, Z.; Cronin, S. B.; Koga, T. *Phys. Solid State* **1999**, *41*, 679−682.
(9) Harman, T. C.; Taylor, P. J.; Spears, D. L.; Walsh, M. P. *J. Electron Mater.* **2000**, *29*, L1−L4.
(10) Hicks, L. D.; Dresselhaus, M. S. *Phys. Rev. B: Condens. Mater. Phys.* **1993**, *47*, 16631−16634.
(11) Ghamaty, S.; Elsner, N. B. *Mater. Res. Soc. Symp. Proc.* **2004**, *793*, S8.13.11−S18.13.14.
(12) Harman, T. C.; Taylor, P. J.; Walsh, M. P.; LaForge, B. E. *Science* **2002**, *297*, 2229−2232.
(13) Dresselhaus, M. S.; Lin, Y. M.; Black, M. R.; Rabin, O.; Dresselhaus, G. *Mater. Res. Soc. Symp. Proc.* **2004**, *793*, S10.14.11−S10.14.12.
(14) Venkatasubramanian, R.; Siivola, E.; Colpitts, T.; O'Quinn, B. *Nature* **2001**, *413*, 597−602.
(15) Heremans, J. P.; Thrush, C. M.; Morelli, D. T.; Wu, M.-C. *Phys. Rev. Lett.* **2002**, *88*, 216801−216804.
(16) Heremans, J.; Thrush, C. M. *Phys. Rev. B: Condens. Mater. Phys.* **1999**, *59*, 12579−12583.
(17) Ritter, J. J. *Inorg. Chem.* **1994**, *33*, 6419−6420.
(18) Ritter, J. J.; Maruthamuthu, P. *Inorg. Chem.* **1995**, *34*, 4278−4280.
(19) Groshens, T. J.; Gedridge, R. W. J.; Lowe-Ma, C. K. *Chem. Mater.* **1994**, *6*, 727−729.
(20) Foos, E. E.; Stroud, R. M.; Berry, A. D. *Nano Lett.* **2001**, *1*, 693−695.
(21) Prieto, A. L.; Sander, M. S.; Martín-González, M. S.; Gronsky, R.; Sands, T.; Stacy, A. M. *J. Am. Chem. Soc.* **2001**, *123*, 7160−7161.
(22) Jin, C.; Xiang, X.; Jia, C.; Liu, W.; Cai, W.; Yao, L.; Li, X. *J. Phys. Chem. B* **2004**, *108*, 1844−1847.
(23) Sander, M. S.; Prieto, A. L.; Gronsky, R.; Sands, T.; Stacy, A. M. *Adv. Mater.* **2002**, *14*, 665−667.
(24) Sapp, S. A.; Lakshmi, B. B.; Martin, C. R. *Adv. Mater.* **1999**, *11*, 402−404.
(25) Ding, Z.; Viculis, L.; Cronin, S.; Koga, T.; Dresselhaus, M.; S.-C.Huang; Kaner, R. B. In *Solution Chemical Routes to Two-dimensional Bismuth Tellurides for Thermoelectric Applications*; Thin Films: Preparation, Characterization, Applications, Proceedings of a Symposium of the ACS; Kluwer Academic/Plenum Publishers: New York, 2002.
(26) Cronin, S. B.; Koga, T.; Sun, X.; Ding, Z.; Huang, S.-C.; Kaner, R. B.; Dresselhaus, M. S. *Mater. Res. Soc. Symp. Proc.* **1999**, *545*, 397−402.

10.1021/ja052286j CCC: $30.25

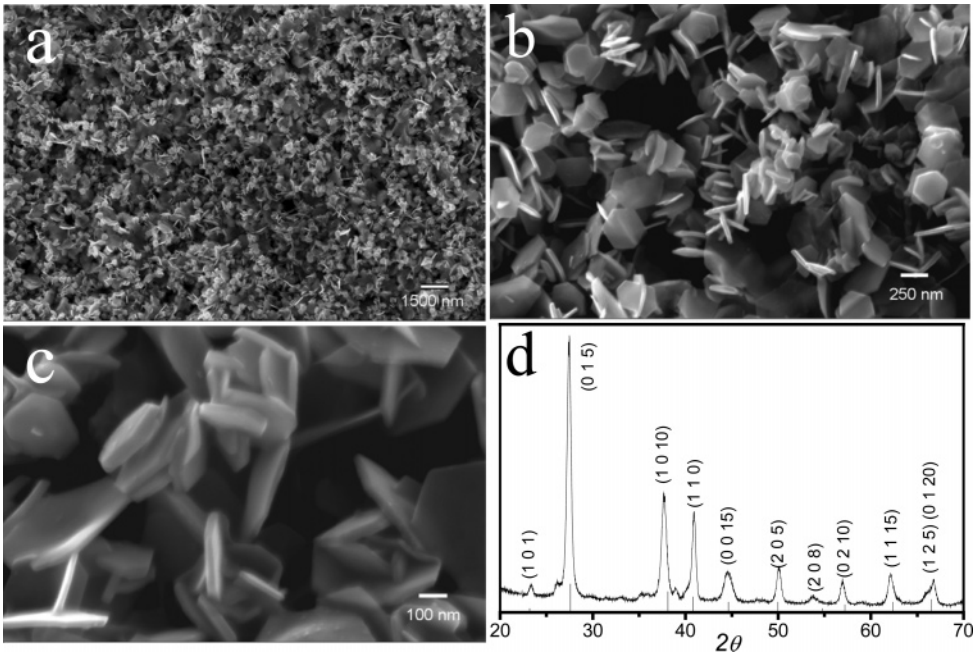

Figure 1. SEM images (a−c) and XRD pattern (d) of Bi_2Te_3 nanoplatelets synthesized in phenyl ether at 150 °C.

ature solution synthesis is a promising approach to achieve high-quality nanocrystals with shape- and size-control.[27−29] On the basis of this strategy, we recently demonstrated our progressive syntheses of PbTe nanocrystals[30] and Mn-doped PbSe nanoarrays.[31] In this contribution, we report the synthesis of Bi_2Te_3 single-crystal hexagonal nanoplatelets, and then, for the first time, we demonstrate a two-step epitaxial growth of the cylindrical strings of Bi_2Te_3 nanoplatelets on the surface of the Te rod by packing them along the *c*-axis in a top−bottom−top−bottom sequence. We realize that it may be feasible to use this structure as a potential thermoelectric building block because the thickness of the Bi_2Te_3 platelet has been confined in such a structure.

Experimental Section

Bi_2Te_3 was synthesized in a hot phenyl ether solution under an argon stream. We employed two precursors: bismuth-2-ethylhexanoate (Alfa Aesar) which was predissolved in octyl ether (0.1 M bismuth), and Te in trioctylphosphine (TOP) which was prepared by dissolving 6.38 g of tellurium ingots (Aldrich, 99.999%) in 100 mL of TOP (Aldrich, 90%) and stirring overnight in a glovebox (0.5 M for Te). In a typical experimental, discrete Bi_2Te_3 nanoplatelets were prepared by rapidly injecting a room-temperature trioctylphosphine telluride (Te−TOP)[30] solution (0.3 mL) into a vigorously stirred hot mixture of 10 mL of phenyl ether and 1 mL of octyl ether solution containing 0.1 M bismuth-2-ethylhexanoate, in the presence of 1.5 mL of oleic acid (90%, Aldrich) at 150 °C in a three-neck flask equipped with a condenser under an argon stream. The formation of Bi_2Te_3 nanoplatelets could be followed by monitoring the color change of the mixture. The color of the phenyl ether containing Bi precursors was initially bright yellow. It gradually turned dark after the Te−TOP solution was injected, indicating the formation of Bi_2Te_3 nanoplatelets. Black products were finally obtained after the mixture was maintained at 150 °C for 30 min. Gray precipitates were isolated after the mixture was washed with centrifugation. Transmission electron microscopy (TEM) observation and energy-dispersive X-ray spectroscopy (EDS) spectra for individual hexagonal nanoplatelets and epitaxially grown structures were conducted using a transmission electron microscope (JEOL 2010) and a field-emission transmission electron microscope (Hitachi 2000 FE-TEM), respectively. The XRD pattern was recorded on an X-ray diffractometer (Philips X-pert system). The microstructure of discrete hexagonal nanoplatelets and epitaxially grown structures were studied using a field-emission scanning electron microscope (LEO 1530 FE-SEM).

Results and Discussion

The as-prepared Bi_2Te_3 platelets were analyzed on a SEM, exhibiting relatively uniform shapes of hexagons on top−bottom facets, and their thickness is in nanometer scale. Panels a−c in Figure 1 show their SEM images in different magnifications. It is estimated that these Bi_2Te_3 hexagonal platelet-like crystals possess a fixed edge in the length of ∼200−300 nm, and the thickness of these platelets is less than ∼15 nm. An XRD pattern of these nanoplatelets was also recorded and demonstrated in Figure 1d. According to the standard ICDD PDF card (No. 08-0021), all of the detected peaks are indexed as those from the rhombohedral Bi_2Te_3 crystal [space group ($R\bar{3}m$)(166)] with hexagonal cells containing three formula units.[32] The possible mechanism of forming such hexagonal Bi_2Te_3 nanoplatelets may be due to its anisotropic structure. The Bi_2Te_3 crystal consists of 15 layers stacked along the *c*-axis and presents the combination of three hexagonal layer stacks of the composition in which each set consists of five atoms (Te_1−Bi−Te_2−Bi−Te_1). The bonding within the Te_1−Bi−Te_2−Bi−Te_1 layer is considered to be covalent, while the bonding between Te_1−Te_1 layers is the *van der Waals forces*. The intrinsic crystal properties dominate the shape of the primary Bi_2Te_3 particles (i.e., platelet seed).[33] Due to this anisotropic bonding environment, the rate

(27) Murray, C. B.; Kagan, C. R.; Bawendi, M. G. *Annu. Rev. Mater. Sci.* **2000**, *30*, 545−610.
(28) Murray, C. B.; Norris, D. J.; Bawendi, M. G. *J. Am. Chem. Soc.* **1993**, *115*, 8706−8715.
(29) Puntes, V. F.; Krishnan, K. M.; Alivisatos, A. P. *Science* **2001**, *291*, 2115−2117.
(30) Lu, W.; Fang, J.; Stokes, K. L.; Lin, J. *J. Am. Chem. Soc.* **2004**, *126*, 11798−11799.
(31) Lu, W.; Gao, P.; Jian, W. B.; Wang, Z. L.; Fang, J. *J. Am. Chem. Soc.* **2004**, *126*, 14816−14821.
(32) Feutelais, Y.; Legendre, B.; Rodier, N.; Agafonov, V. *Mater. Res. Bull.* **1993**, *28*, 591−596.

of crystal growth along the top−bottom crystalline planes should be much greater than that along *c*-axis, which is perpendicular to these top−bottom planes as the crystalline facets tend to develop on the low-index planes to minimize the surface energy when growing. Stabilizing agent (i.e., oleic acid) capped on the surfaces of Bi_2Te_3 nanocrystals may further enlarge the energetic difference between the top−bottom facets (large surfaces) and the side facets (small surfaces, which are parallel to the *c*-axis). Although the concentration of reactants and stabilizing agent are also the parameters to control the nanoplatelet formation, it seems that temperature is the key factor which affects the morphology of Bi_2Te_3 nanoplatelets. Low reaction temperature results in much thinner platelets but in irregular shapes of the top−bottom facets; whereas high reaction temperature gives more uniform hexagonal platelets on top−bottom facets, but thick platelets. Actually, the shape and thickness of these nanoplatelets can be tuned by varying the growth temperature.

As demonstrated in Figure 2a, TEM shows the morphology of hexagonal Bi_2Te_3 platelets. The ripple-like patterns are due to the strain resulting from the bend of super-thin nanoplatelets.[34] The corresponding selected-area electron diffraction (SAED) pattern (Figure 2b) can be identified as the [0001] zone axis projection of the hexagonal Bi_2Te_3 reciprocal lattice. The top−bottom surfaces are {0001} facets, whereas the six side surfaces are $\{11\bar{2}0\}$ facets. The diffraction observation indicates that $\langle 11\bar{2}0\rangle$ is the growth directions for developing the hexagonal crystals and that the as-prepared Bi_2Te_3 nanoplatelets are single-crystal and dominated by {0001} facets. Corresponding high-resolution TEM images (only one shown in Figure 2c) of selected areas of Bi_2Te_3 nanoplatelets confirm that the nanoplatelets are single crystal and defect-free, and that ⟨0001⟩ is the slowest growth direction. EDS spectrum (Figure 2d) taken from the Bi_2Te_3 nanoplatelets further confirms the compositions of Bi_2Te_3.

Bismuth selenide (Bi_2Se_3) possesses a crystal structure the same as that of Bi_2Te_3. Since we have successfully synthesized hexagonal Bi_2Se_3 nanoplatelets[35] by employing a similar approach mentioned above (images are not shown) and it was also reported that hexagonal platelet-like Bi_2Se_3 crystals could be prepared via a hydrothermal process,[36] we have further introduced selenium as a minor component into the current solution system by adding ∼5% (mol %) of selenium−trioctylphosphine (Se-TOP) solution[31] at 200 °C and conducting a similar high-temperature solution reaction and posttreatment. The objectives of this work are two-fold: (1) to structurally obtain well-orientated Bi_2Te_3 arrays of nanoplatelets with an epitaxial growth perpendicular to *c*-axis and (2) to achieve *n*-type Bi_2Te_3 nanocrystals due to their highly stable thermoelectric figure of merit,[37] as the *n*-type Bi_2Te_3 can be obtained by doping selenium in low percentages into pure Bi_2Te_3. We have carefully examined the original product using high-resolution SEM, showing that a composite nanostructure of Te and Bi_2Te_3 was formed during the growth. About 30−40% of the products were epitaxially grown into well-defined one-dimensional (1D) strings

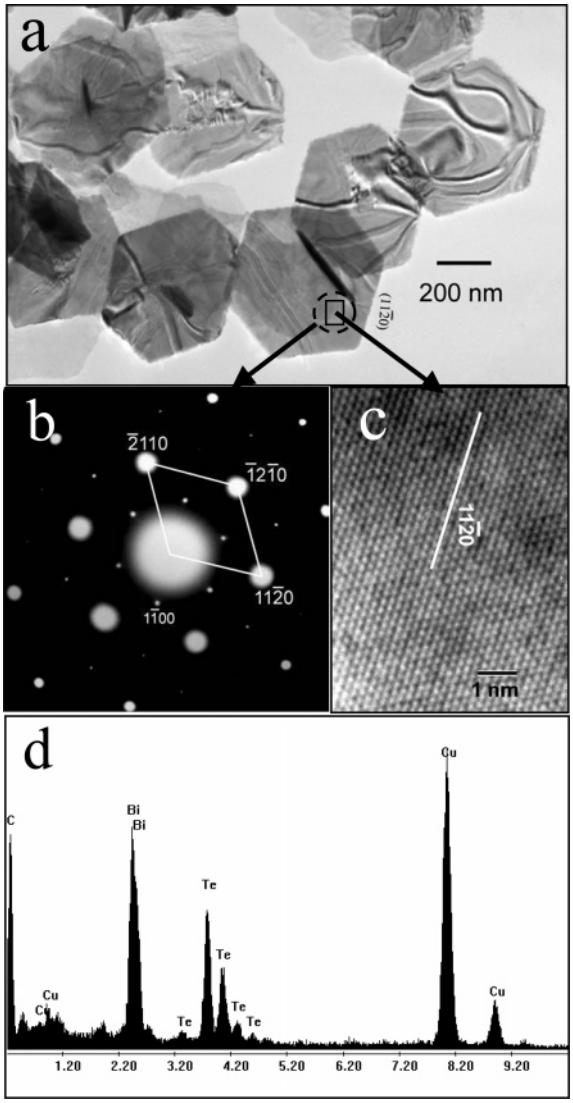

Figure 2. TEM image of Bi_2Te_3 nanoplatelets (a), electron diffraction pattern on a Bi_2Te_3 nanoplatelet (b), high-resolution TEM image of a selected area on a Bi_2Te_3 nanoplatelet (c), and EDS of Bi_2Te_3 nanoplatelets showing that the average atomic ratio of compositions Te to Bi is about 58.69:41.31 (d).

of pure Bi_2Te_3 nanoplatelets in which the top-bottom planes of Bi_2Te_3 nanoplatelets are perpendicular to the *c*-axis of the central rod (see Figure 3a), and 60−70% of them still remained in individual hexagonal nanoplatelets under the current experimental conditions. A size-selective precipitation can be further applied to this system using a pair of solvents consisting of toluene and ethanol to refine and isolate the 1D aligned Bi_2Te_3-composite strings.

Figure 3a exhibits an SEM image that displays many strings of platelet structures. The strings are made of the platelets presented in Figure 3 but with a well-controlled orientation relationship. A close examination of the strings indicates that the platelets grow out of a rod and they are mostly attached to the edge of a main body, indicating a possible two-step growth process of the nanostructure (Figure 3b, c), which will be discussed later. TEM image presents the ordered and aligned arrangement among the platelets (Figure 3d), which suggests a possible crystallographic orientation relationship among them.

The local chemical composition and crystallographic relationship between the nanoplatelets and rod have been analyzed by

(33) Hollingsworth, J. A.; Poojary, D. M.; Clearfield, A.; Buhro, W. E. *J. Am. Chem. Soc.* **2000**, *122*, 3562−3563.
(34) Kong, X. Y.; Ding, Y.; Yang, R.; Wang, Z. L. *Science* **2004**, *303*, 1348−1351.
(35) Unpublished.
(36) Wang, D.; Yu, D.; Mo, M.; Liu, X.; Qian, Y. *J. Cryst. Growth* **2003**, *253*, 445−451.
(37) Yamashita, O.; Tomiyoshi, S. *J. Appl. Phys.* **2004**, *95*, 6277−6283.

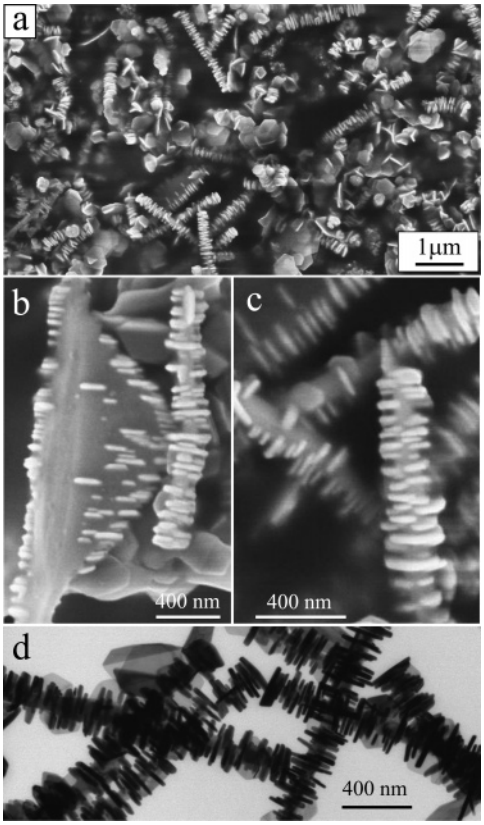

Figure 3. Low-magnification (a), high-magnification (b, c) SEM images, and TEM image (d) of the aligned platelet structure.

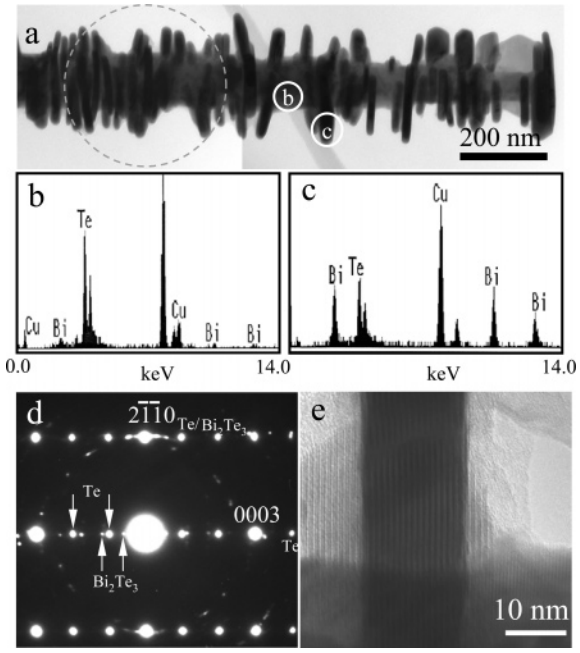

Figure 4. TEM image (a), corresponding EDS spectra (b, c) acquired from the circled areas of b and c in (a). Electron diffraction patterns recorded from the area enclosed by the dashed circle in (a), showing epitaxial orientation relationship between the platelets (Bi_2Te_3) and the matrix (Te). High-resolution TEM image (e) recorded from the structure shown in (a). In the circled area of b, average atomic ratio of Te to Bi is around 98.04: 1.96, whereas in the circled area of c, that of Te to Bi is around 53.60: 46.40.

EDS. The EDS spectra in Figure 4b and c were collected from the circles enclosed area b and c in Figure 4a, respectively. Unlike that of the nanoplatelets, as depicted in the captions of Figure 4, the content of Bi in the rod is so low that it can be neglected, indicating that the rod is Te and the platelets are Te−Bi compound. The SAED pattern recorded from the circled area indicated in Figure 4a clearly presents the epitaxial orientation relationship among the rod and the platelets (Figure 4d). Detailed analysis of the diffraction pattern shows the presence of hexagonal structured Te and rhombohedral Bi_2Te_3. The weak diffraction spots indicated by arrowheads are indexed using the Bi_2Te_3 structure, which are coming from the nanoplatelets. Tellurium has hexagonal structure with $a = 0.4312$ nm and $c = 0.5957$ nm [XRD ICDD PDF card No. 85-0557, space group $P3{\cdot}21$ (152)]. As mentioned before, Bi_2Te_3 has rhombohedral structure with hexagonal cells of $a = 0.4384$ nm and $c = 3.045$ nm.[32] A HRTEM image including both the rod and nanoplatelet is given in Figure 4e, implying that the *c*-axis of Bi_2Te_3 nanoplatelet is parallel to the *c*-axis of the Te rod. The crystallographic orientation between Te rod and Bi_2Te_3 nanoplatelets can be described as $(0001)_{Te}||(0001)_{Bi2Te3}$, $[2\bar{1}\bar{1}0]_{Te}||[2\bar{1}\bar{1}0]_{Bi2Te3}$. Considering the crystal structures of Bi_2Te_3 and Te, the lattice mismatch between Te and Bi_2Te_3 is 1.67%, the mismatch between $(0001)_{Te}$ and $(0006)_{Bi2Te3}$ is 14.4%; thus, it is possible to have a long distance epitaxial growth of Bi_2Te_3 on Te, but the growth along [0001] is limited due to the large lattice mismatch, possibly resulting in the formation of platelet Bi_2Te_3 on Te rod. On the other hand, the Bi_2Te_3 platelets are separated from each other from the top face to the bottom face due to the relatively high surface energy resulting from the anisotropic bonding environment mentioned above. EDS results do not show the element Se on a detectable level from the solid products. However, we did qualitatively determine the trace of Se from the original reaction solution using an inductively coupled plasma (ICP) technique. Although the mechanism associated with the formation of Te in this process is still ambiguous, we propose a possible explanation as follows: when metal Te or Se is dissolved in TOP, the metal−TOP complex may be present in the solution due to the fact that lone-pair electrons of phosphine tend to fill the p-orbital of the metal. However, when Te−TOP and Se−TOP complexes coexist at high temperature, the tellurium (with enriched electron) from Te−TOP complex may be "oxidized" and recovered into metallic state. This is because the atomic radius of Te atom is much larger than that of Se atom, meaning that the capability of accepting electrons for metal Te is much weaker than that for Se (this is also the reason metal Se is much easier to dissolve in TOP than Te is). As a result, a small amount of metallic Te is precipitated out, and the Se−TOP complex becomes more stable in the high-temperature Bi-containing organic solution when both Te−TOP (major component) and Se−TOP (minor component) are mixed. This explanation can also be supported by the standard reduction potentials of both metals in aqueous solution at room temperature[38] ($Te + 2 \rightarrow Te^{2-}$, $E^\circ = -1.143$ V; $Se + 2 \rightarrow Se^{2-}$, $E^\circ = -0.924$ V).

Conclusions

Combining the structural information provided above, a growth process can be proposed about the formation of the nanostructure. The growth is suggested to be a two-step process. The first step is the formation and fast growth of the Te nanorod

(38) Meites, L., Ed. *Handbook of Analytical Chemistry*, 1st ed.; McGraw-Hill Book Company: New York, 1969.

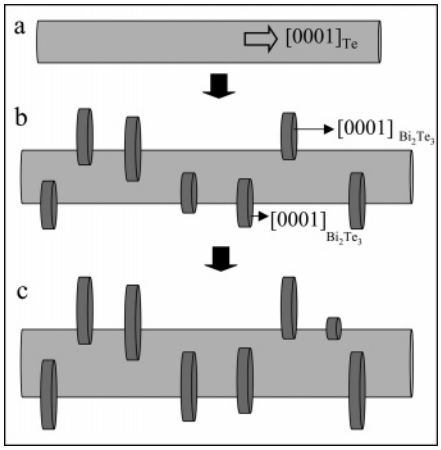

Figure 5. Proposed growth process of the Bi_2Te_3−Te nanostructure.

along [0001] (Figure 5a), followed by a nucleation and epitaxial growth of the Bi_2Te_3 nanoplatelets (Figure 5b). The epitaxial orientation relationship is preserved to reduce the lattice mismatch energy. Further growth of the platelets perpendicular to the axial direction forms the structure of Bi_2Te_3 nanoplatelets partially embedded in Te matrix (Figure 5c). In conclusion, single-crystal, defect-free, and hexagonal Bi_2Te_3 nanoplatelets have, for the first time, been synthesized in organic solution at 150 °C, in the presence of oleic acid. With the introduction of a small amount of Se−TOP precursor at 200 °C, these pure Bi_2Te_3 hexagonal nanoplatelets can be epitaxially grown on surface of each Te rod to form strings of platelet structures due to a minimum mismatch of $(0001)_{Te}||\ (0001)_{Bi2Te3}$ and $[2\bar{1}\bar{1}0]_{Te}\ ||\ [2\bar{1}\bar{1}0]_{Bi2Te3}$ and relatively high surface energy on the top-bottom facets of Bi_2Te_3 nanoplatelets. In this epitaxial growth, the *c* direction of Bi_2Te_3 nanoplatelet is parallel to the *c*-axis of the Te rod. After size-selective posttreatment, it is possible to refine and isolate the single component of 1D aligned strings of Bi_2Te_3 nanoplatelets by separating and removing the individual Bi_2Te_3 nanoplatelets. These well-built 1D structures containing phase boundaries on nanofacets are desired low-dimensional thermoelectric building-blocks for possibly achieving a high thermoelectric figure of merit.

Acknowledgment. This work was supported by BSST LLC, NSF CAREER Program (DMR-0449580), NSF NIRT Program (ECS-0210332), and NASA Vehicle System Program.

JA052286J